Electron–hydrogen-atom elastic and inelastic scattering with screened Coulomb interaction around the $n = 2$ excitation threshold

Song Bin Zhang,[1] Jian Guo Wang,[2] and R. K. Janev[3]

[1]*Hefei National Laboratory for Physical Sciences at Microscale and Department of Modern Physics, University of Science and Technology of China, Hefei 230026, People's Republic of China*

[2]*Key Laboratory of Computational Physics, Institute of Applied Physics and Computational Mathematics, P. O. Box 8009, Beijing 100088, People's Republic of China*

[3]*Macedonian Academy of Sciences and Arts, P. O. Box 428, 1000 Skopje, Macedonia*

(Received 15 January 2010; published 25 March 2010)

The effects of Coulomb interaction screening on electron–hydrogen-atom elastic and excitation scattering around the $n = 2$ threshold have been investigated by using the R-matrix method with pseudostates. The elastic and excitation collision strengths show dramatic changes when the interaction screening length D varies from ∞ to 3.8 a.u., as a result of the convergence of $^{1,3}S$ Feshbach resonances to the varying $2s$ threshold and of the transformation of $^{1,3}P$ and ^{1}D Feshbach resonances into shape-type resonances when they pass across the $2s$ and $2p$ threshold at certain critical value of D, respectively [S. B. Zhang *et al.*, Phys. Rev. Lett. **104**, 023203 (2010)]. The resonance parameters for a large number of D in the range $D = \infty$–3.8 a.u. are presented. It is observed that the $^{1,3}P$ and ^{1}D resonance contributions to the elastic and excitation collision strengths decrease rapidly with decreasing D after the resonance passes the critical D value. The contribution of a $^{1}S^{e}$ Feshbach resonance to the elastic or excitation collision strength changes into a cusp after the resonance merges into its parent $2s$ state and immerses into the background with the further decrease of D.

DOI: 10.1103/PhysRevA.81.032707 PACS number(s): 34.80.Dp, 52.20.Fs

I. INTRODUCTION

In many physical systems (dense plasmas, electrolytes, solid-state matter) the Coulomb interaction between the constituent charged particles becomes screened due to the correlated many-particle interactions [1–3]. To the lowest particle correlation order (pairwise correlations), the Coulomb interaction screening reduces to the Debye-Hückel (Yukawa-type) potential. For the interaction of an ion of charge Z with an electron it has the form [1–3]:

$$V(r) = -\frac{Ze^2}{r}\exp\left(-\frac{r}{D}\right), \tag{1}$$

where D is the screening length. In a plasma, $D = (k_B T_e/4\pi e^2 n_e)^{1/2}$, with T_e and n_e being the plasma electron temperature and density, respectively, and k_B is the Boltzmann constant. Obviously, in other many-particle systems, the relation of the screening length to the parameters of the system may have a different form.

In the context of hot, dense plasmas studies, a number of theoretical investigations of atomic collision processes have been carried out by using the interaction (1). Among those involving electron impact, studies for the electron–hydrogen-like ion excitation [4–8] and ionization [9] performed, mainly within the Born and two-state close-coupling approximations. These studies, however, have not addressed the question of the effects of screened Coulomb interaction on the resonances around the thresholds of excitation processes. These effects have been investigated only recently [10] for the $1s \rightarrow 2s$ and $1s \rightarrow 2p$ excitation in electron–hydrogen-atom collisions around the $n = 2$ resonant energy region by employing the R-matrix method with pseudostates (RMPS).

The most prominent features of the potential (1) is the lifting of the Coulomb l degeneracy of hydrogenic energy levels and the finite number of bound states supported by the potential for any finite value of D (see, e.g., Ref. [11]). The hydrogenic n-threshold now splits into n components, the energy difference between which increases with decreasing the screening length D [12]. The finite number of bound states in the potential (1) implies that with decreasing D the binding energies of nl states decrease and the nl energy levels successively enter in the continuum at certain critical screening values D_{nl}. The numerical solution of Schrödinger equation with the potential (1) [12] shows that the following relations for D_{nl} hold (at least up to $n = 7$): $D_{n+1,l} > D_{nl}$ and $D_{n,l+1} > D_{nl}$. In the context of the present work we should also emphasize that with decreasing D the excitation threshold energies also decrease. For a given n, the states with a lower l value have lower thresholds for any fixed value of D. As a consequence of the decrease of energies of bound states when D decreases, the corresponding wave functions become increasingly more diffuse, with obvious effects on the near-threshold processes. We also mention that for the $1s$, $2s$, and $2p$ states, considered in the present article, the D_{nl} values are 0.840, 3.223, and 4.541 atomic units, respectively [12].

In the present article we shall study the effects of the Coulomb interaction screening on the elastic and excitation collision strengths in electron–hydrogen-atom collisions in energy region around the $n = 2$ thresholds by employing the R-matrix method with pseudostates. The energy positions and widths of resonances that characterize the elastic and excitation processes in this region will be calculated for a large number of D values in the range ∞–3.8 atomic units that allows us to follow the dynamical evolution of collision strengths when D varies. The effects of the phenomenon of crossover of Feshbach into shape-type resonances at certain critical values of D [10] on the behavior of elastic and excitation collision strengths will also be investigated in greater detail.

The organization of the article is as follows. In the next section we describe the method of our RMPS calculations with the interaction in the form (1), select the expansion basis for different D, and perform a test of the sufficiency of the basis for the collision case without screening. In Sec. III we present the results of our calculations for the resonant parameters for different values of D in the range $D = \infty$–3.8 atomic units. In Sec. IV we present and discuss the results of our calculation for $1s \rightarrow 2s$, $1s \rightarrow 2p$ excitation, and $1s \rightarrow 1s$ elastic collision strengths, and in Sec. V we give our conclusions.

Atomic units will be used if otherwise not stated explicitly.

II. METHOD OF CALCULATIONS

A. RMPS with screened Coulomb interaction

The R-matrix method for electron-atom collisions has been discussed in details by Burke *et al.* [13,14]. In an R-matrix calculation, the configuration space is partitioned into three regions: an internal region, an external region, and an asymptotic region. In the internal region, the electron exchange and correlation effects between the incident and target electrons are important and the $(N+1)$-electron complex behaves in a way similarly to a bound system. Consequently, the total wave function of the $N+1$ electron system is expanded in a configuration interaction (CI) basis which takes the following form for each total orbital angular momentum (L), spin (S), and parity (π) (in the nonrelativistic scattering these quantum numbers are conserved):

$$\psi_k^{LS\pi}(\mathbf{X}_{N+1}) = \widehat{\mathrm{A}} \sum_{ij} \overline{\phi}_i^{LS\pi}(\mathbf{X}_N; \hat{r}_{N+1}\boldsymbol{\sigma}_{N+1}) r_{N+1}^{-1} u_{ij}(r_{N+1}) \times a_{ijk}^{LS\pi} + \sum_j \chi_j^{LS\pi}(\mathbf{X}_{N+1}) b_{jk}^{LS\pi}, \tag{2}$$

where $\widehat{\mathrm{A}}$ is the antisymmetrization operator which accounts for electron exchange between the target electrons and the free electron. The functions $\overline{\phi}_i^{LS\pi}$ are formed by coupling the target states with the spin-angle functions of the scattered electron, u_{ij} are radial basis functions representing the scattered electron, and $\chi_j^{LS\pi}$ are square-integrable (L^2) correlation functions. The coefficients $a_{ijk}^{LS\pi}$ and $b_{jk}^{LS\pi}$ are obtained by diagonalizing the $(N+1)$-electron Hamiltonian in the basis $\psi_k^{LS\pi}$.

The $(N+1)$-electron nonrelativistic Hamiltonian with the interaction potential (1) has the form:

$$H^{N+1} = \sum_{n=1}^{N+1} \left[-\frac{1}{2}\nabla_n^2 - \frac{Z}{r_n}\exp(-r_n D^{-1}) + \sum_{m>n}^{N+1} \frac{1}{r_{mn}} \exp(-r_{mn} D^{-1}) \right], \tag{3}$$

where $\mathbf{r}_n$ is the electron radius vector with respect to the atomic nucleus having charge Z, $r_{mn} = |\mathbf{r}_m - \mathbf{r}_n|$ is the interelectron distance and D is the interaction screening length. The electron-electron interaction term in Eq. (3) can be expanded as [15]:

$$V_{ee} = \frac{\exp(-r_{mn}D^{-1})}{r_{mn}} = \begin{cases} \sum_{\lambda=0}^{\infty} \frac{r_<^\lambda}{r_>^{\lambda+1}} P_\lambda(\cos\theta_{mn}) & D^{-1} = 0 \\ -D^{-1} \sum_{l=0}^{\infty} (2\lambda+1) j_\lambda(iD^{-1}r_<) h_\lambda^{(1)}(iD^{-1}r_>) P_\lambda(\cos\theta_{mn}) & D^{-1} > 0 \end{cases}, \tag{4}$$

where $r_> = \max(r_m, r_n)$, $r_< = \min(r_m, r_n)$, P_l, j_l and $h_l^{(1)}$ are the Legendre polynomials, spherical Bessel functions, and spherical Hankel functions of the first kind with complex arguments, respectively.

In the external region, the electron exchange and correlation effects between the incident and target electrons are negligible. The scattered electron then moves in the long-range local multipole potential of the target atom (or ion). The reduced radial wave functions, $F_i(r)$, describing the motion of scattered electron, satisfy a set of coupled second-order differential equations:

$$\left[\frac{d^2}{dr^2} - \frac{l_i(l_i+1)}{r^2} + \frac{2(Z-N)}{r}\exp\left(-\frac{r}{D}\right) + k_i^2\right] F_i(r) = 2\sum_{\lambda=1}^{\lambda_{\max}} \sum_{j=1}^{n} \frac{a_{ij}^\lambda}{r^{\lambda+1}} F_j(r), \quad r > a_0. \tag{5}$$

Here $(Z-N)$ is the residual target charge, n is the number of channel functions, l_i and k_i^2 are the channel angular momentum and energy, respectively, a_0 is the boundary of the internal region, and the long-range potential coefficients a_{ij}^λ is:

$$a_{ij}^\lambda = \begin{cases} \langle\overline{\phi}_i| \sum_{m=1}^{N} r_m^\lambda P_\lambda(\cos\theta_{m,N+1}) |\overline{\phi}_j\rangle & D^{-1} = 0 \\ -D^{-1} a_0^{\lambda+1} \langle\overline{\phi}_i| \sum_{m=1}^{N} (2\lambda+1) j_\lambda(iD^{-1}r_m) h_\lambda^{(1)}(iD^{-1}a_0) P_\lambda(\cos\theta_{m,N+1}) |\overline{\phi}_j\rangle & D^{-1} > 0 \end{cases}. \tag{6}$$

We note that the interaction V_{ee} for $D^{-1} > 0$ cannot be expanded in multipoles exactly. At the boundary of the internal region a_0, however, this expansion can be considered as an adequate approximation, since (*i*) at $a_0 V_{ee}$ is small and (*ii*) it also provides a smooth connection of V_{ee} at the boundary a_0.

For the neutral atom, the residual target charge is $(Z\text{-}N) = 0$, so the boundary conditions in the asymptotic region are:

$$F_{ij} \underset{r\to\infty}{\sim} \begin{cases} k_i^{-1/2}(\sin\theta_i \delta_{ij} + \cos\theta_i K_{ij}) & \text{open channels} \\ \exp(-\varphi_i)\delta_{ij} & \text{closed channels} \end{cases}, \quad (7)$$

where the second index j on F_{ij} denotes the linear independent solutions of Eq. (5), $\theta_i = k_i r - \frac{1}{2} l_i \pi$, $\varphi_i = |k_i| r$, and K_{ij} are the elements of the real symmetric K matrix. The S and T matrices are then defined in terms of the K matrix by

$$\mathbf{S} = (\mathbf{1} - i\mathbf{K})^{-1}(\mathbf{1} + i\mathbf{K}), \qquad \mathbf{T} = \mathbf{S} - \mathbf{1}. \quad (8)$$

The partial collision strength for a transition from an initial state $\alpha_i L_i S_i$ to a final target state $\alpha_j L_j S_j$, where α_i and α_j represent the additional quantum numbers necessary to completely define the target states, is given by

$$\Omega_{ij}^{LS\pi} = \frac{(2L+1)(2S+1)}{2} \sum_{l_i l_j} |T_{ij}|^2, \quad (9)$$

and the total collision strength is given by

$$\Omega_{ij} = \sum_{LS\pi} \Omega_{ij}^{LS\pi}. \quad (10)$$

The total cross section for the transition $i \to j$ is related to Ω_{ij} by

$$\sigma_{i\to j} = \frac{\pi a_0^2}{k_i^2 (2L_i + 1)(2S_i + 1)} \Omega_{ij}. \quad (11)$$

The physical orbitals of hydrogen atom with the screened Coulomb potential (1) have been calculated by the piecewise exact power series expansions of the radial function [16], while the pseudo-orbitals have been optimized by the CIV3 computer code [17]. The used R-matrix code is a modified version based on the Belfast [18,19] atomic R-matrix packages in which the Coulomb interactions in the $(N+1)$-electron nonrelativistic Hamiltonian are replaced by Yukawa-type screened Coulomb interactions.

The resonance parameters have been determined by fitting the eigenphase sum to the Breit-Wigner form:

$$\delta(E) = \delta_0(E) + \tan^{-1}\left(\frac{\Gamma/2}{E_r - E}\right), \quad (12)$$

where E_r is the resonance position, Γ is the total width, and $\delta_0(E)$ is the background phase near the resonance. When the background varies slowly over the resonance profile, Γ can be determined from the relation [20]:

$$\Gamma = 2/\delta'(E_r). \quad (13)$$

In the general case, the point of maximum gradient $\delta'(E)$ serves as definition for the position of the resonance, and the width can be determined from Eq. (13). As in the case of the shape resonance $^1P^\circ$ of H^-, the rapidly decreasing phase can greatly distort or even destroy any resonance structure, rendering it extremely difficult to ascertain whether a resonance is actually there [21]. For such situations, an appropriate fitting method has been proposed by Callaway [22,23] which employs the relation

$$\delta(E) = \frac{a}{E - E_{th}} + b + c(E - E_{th}) + \tan^{-1}\left(\frac{\Gamma/2}{E_r - E}\right). \quad (14)$$

In our calculations we have used an energy grid of 10^{-5} Ry throughout the energy region considered, but in the vicinity of narrow resonances we have refined it to 10^{-6} Ry or even 10^{-7} Ry in order to determine accurately the resonance parameters.

B. Calculations for the unscreened case: test of the sufficiency of expansion basis

In order to check the sufficiency of the basis set used in our RMPS calculations, we have first considered the unscreened case by using 14 physical states ($1s - 5s, 2p - 5p, 3d - 5d, 4f, 5f$) and four pseudostates ($6\bar{s}, 6\bar{p}, 6\bar{d}, 6\bar{f}$) in the expansion (2) and calculated the $1s \to 1s$ elastic collision strengths and resonance parameters below the $n = 2$ excitation threshold, and the $1s \to 2s$ and $1s \to 2p$ excitation collision strengths between the $n = 2$ and $n = 3$ excitation thresholds. The results for the resonance parameters agree very well with the variational results of Gien [24] and with the three eigenstate expansion (supplemented by correlation terms) of Burke *et al.* [25] (see Table I). The calculated results for the elastic collision strengths are shown in Fig. 1 (upper panel) and they agree very well with hyperspherical close-coupling calculation of Chen *et al.* [26], as well as with the direct numerical calculations of Wang *et al.* [27]. In the lower panel of Fig. 1 the collision strengths for the $1s \to 2s$ and $1s \to 2p$ transitions of present calculations are given, showing a very good agreement with the 18-state variational results of Callaway [23], the benchmark calculations of Bartschat *et al.* [28] (using the convergent close coupling, RMPS, and intermediate energy R-matrix methods), and with the experimental data of Williams [29]. It should be noted that the fitted position of the $^1P^\circ$ shape resonance (not included in Table I) is lower than that of Callaway [22,23] by 10^{-4} Ry only, but the general agreement is quite good.

TABLE I. Energy (E_r (eV)) and width (Γ (meV)) of Feshbach resonances converging on the n = 2 threshold. The energy conversion 1 Ry = 13.605825 eV.

	Present(14 + 4)		Gien [24]		Bruke *et al* [25]	
$^{2s+1}L^\pi$	E_r	Γ	E_r	Γ	E_r	Γ
$^1S^e$	9.557	48.3	9.558	47.24	9.560	47.5
	10.176	2.48	10.177	2.43	10.178	2.19
	10.203	0.16	10.203	0.14		
$^3S^e$	10.147	0.02	10.147	0.02	10.150	0.02
	10.203	–	10.201	0.001		
$^1P^\circ$	10.176	0.04	10.176	0.04	10.177	0.04
$^3P^\circ$	9.739	5.88	9.738	5.83	9.740	5.94
	10.193	0.14	10.193	0.13		
$^1D^e$	10.125	8.65	10.126	8.58	10.125	8.8

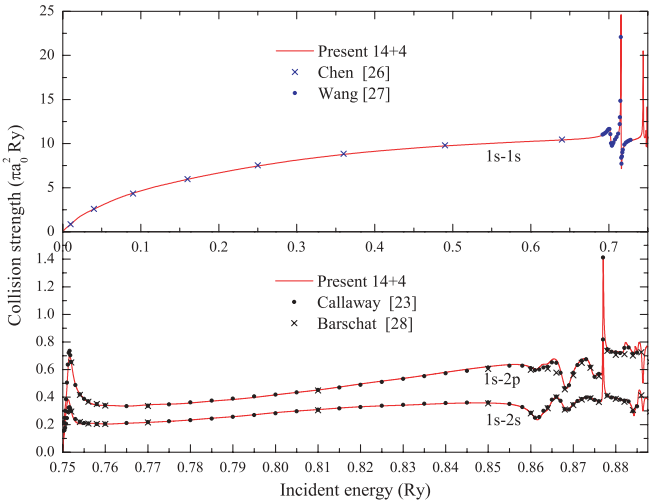

FIG. 1. (Color online) Collision strengths for the unscreened case. Upper panel: $1s$-$1s$ elastic collision strength below n = 2 excitation threshold; lower panel: $1s \rightarrow 2s$ and $1s \rightarrow 2p$ excitation collision strength between the n = 2 and n = 3 excitation thresholds. Red lines: present RMPS results (14 physical states + 4 pseudostates); black dots: 18-state basis variational calculations of Callaway [23]; black cross dots: RMPS results from the benchmark calculation of Bartschat *et al* [28]; blue dots: direct numerical calculations of Wang *et al* [27]; blue cross dots: hyperspherical close-coupling calculation of Chen *et al* [26].

C. Selection of the basis for finite screening lengths

As mentioned in the Introduction, the finite number of bound states supported by the potential (1) for a finite value of the screening length D implies that with decreasing D the energies of bound nl states decrease and for certain critical values D_{nl} they merge with the continuum edge. For instance, the D_{nl} values for the $5l$ states, included in our basis for the unscreened case, lie in the range 19.772 a.u. (for $5s$) to 28.257 a.u. (for $5f$) [12]. For the $4l$ states, this range is 12.687 a.u. (for $4s$) to 20.068 a.u. (for $4f$), while for the $3s$, $3p$, and $3d$ states, the D_{nl} values are 7.171, 8.872, and 10.947 a.u., respectively [12]. Obviously, with decreasing of D below 28 a.u., the states that have already merged with the continuum edge have to be omitted from the part of physical states in the basis adopted for the unscreened case (see the previous subsection). It is also intuitively clear that it would be natural to include in the pseudostate part of the basis the states that have already merged with the continuum. Therefore, with decreasing of D, the number of the physical states included in the basis will gradually decrease, whereas that of pseudostates should increase. In the context of the present study, the lowest limits of the decrease of D are determined by the critical values $D_{2s} = 3.223$ a.u. and $D_{2p} = 4.541$ a.u. at which the $2s$ and $2p$ states merge with the continuum [12] and below which the $1s \rightarrow 2l$ transition does not exist.

By checking the convergence of the results for each value of D for which the RMPS calculations have been performed, we have arrived at the basis sets given in Table II for different groups of D values. The accuracy of calculated results with these basis sets is on the level of that for the unscreened case considered in the previous subsection. We should note that when approaching the D_{2l} values from above, the energy of corresponding states becomes increasingly small, its wave function extends to increasingly large distances, and the backward integration from the asymptotic region toward the inner region becomes increasingly unstable. This results in practical limits to the lowest values of D which for the $2s$ and $2p$ state is 3.8 and 4.6 a.u., respectively.

III. RESONANCE PARAMETERS

The most pronounced resonances around the $n = 2$ threshold region in the unscreened case are the $^1S^e(1,2,3)$, $^3S^e$,$^1P^\circ(1)$, $^3P^\circ(1,2)$, $^1D^e$ Feshbach resonances and the $^1P^\circ(2)$ shape resonance, and these have been thoroughly studied in the past. (The resonance with a given symmetry having a larger number in the parentheses is closer to the threshold.) We have calculated the energy positions and widths of these resonances by using Eqs. (12)–(14). The variation of the resonance positions and $1s \rightarrow 2s$, $1s \rightarrow 2p$ excitation energies when the screening length decreases from $D = \infty$ to $D = 3.8$ a.u. is shown in Fig. 2. The figure shows that as the interaction screening increases the resonance positions and the $1s \rightarrow 2s$, $1s \rightarrow 2p$ excitation energies decrease. This is a consequence of the fact that the gradient of the decrease of the binding energy of $1s$ state when D decreases is larger than that for the energies of $2s$ and $2p$ states. Figure 2 also shows that the resonances disappear when D deceases, and at $D = 3.8$ a.u., only the resonances $^1S^e(1)$ and $^1P^\circ(1)$ remain in the resonance spectrum (see also Fig. 3 and Table III below).

TABLE II. Basis preparation for the R-matrix calculation for various screening length.

Screening Length	Basis
$\geqslant$34	14 physical states ($1s$-$5s$, $2p$-$5p$, 3 d-5 d, $4f$, $5f$) plus 4 pseudostates ($6s$, $6p$, 6 d, $6f$)
30–22	10 physical states ($1s$-$4s$, $2p$-$4p$, 3 d, 4 d, $4f$) plus 4 pseudostates ($5s$, $5p$, 5 d, $5f$)
21,20	9 physical states ($1s$-$4s$, $2p$-$4p$, 3 d, 4 d) plus 5 pseudostates ($4f$, $5s$, $5p$, 5 d, $5f$)
19,18	8 physical states ($1s$-$4s$, $2p$-$4p$, 3 d) plus 6 pseudostates (4 d, $4f$, $5s$, $5p$, 5 d, $5f$)
17–12	6 physical states ($1s$-$3s$, $2p$, $3p$, 3 d) plus 8 pseudostates (4 l, 5 l, ($l = s, p, d, f$))
11,10	5 physical states ($1s$-$3s$, $2p$, $3p$) plus 7 pseudostates (3 d, 4 l, 5 l, ($l = s, p, d, f$))
9	4 physical states ($1s$-$3s$, $2p$) plus 8 pseudostates ($3p$, 3 d, 4 l, 5 l, ($l = s, p, d, f$))
8–4.6	3 physical states (1 s, $2s$, $2p$) plus 9 pseudostates (3 l, 4 l, 5 l, ($l = s, p, d, f$))
4.55–3.8	2 physical states ($1s$, $2s$) plus 7 pseudostates ($2p$, 3 l, 4 l, ($l = s, p, d, f$))

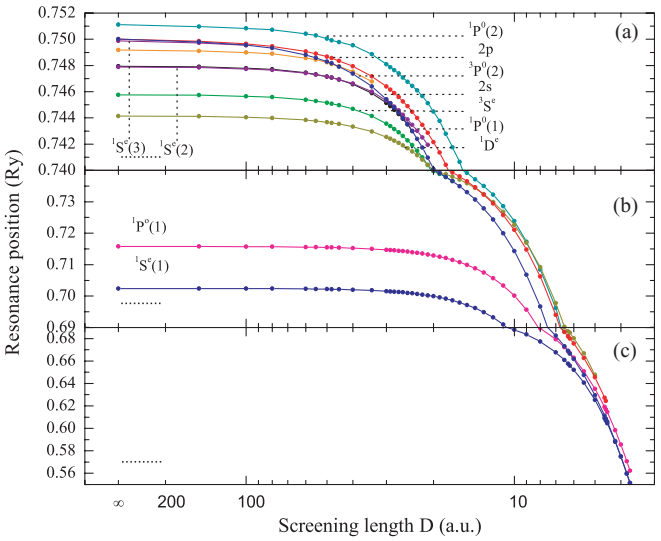

FIG. 2. (Color online) Variation of the positions of Feshbach and shape resonances and of the $1s \rightarrow 2s$, $1s \rightarrow 2p$ excitation energies when the screening length decreases.

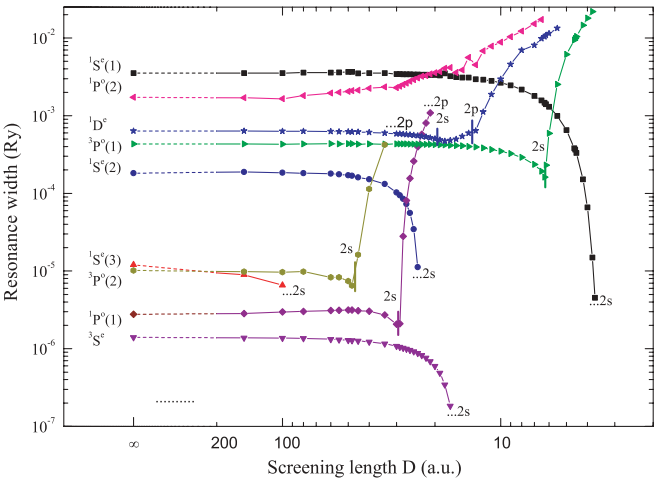

FIG. 3. (Color online) Variation of the widths of Feshbach and shape resonances when the screening length decreases. Short dashed lines represent the critical values of D where Feshbach resonances pass across the $2s$ or $2p$ threshold.

The variation of resonance widths with D is shown in Fig. 3. The figure shows that with decreasing D, the widths of $^{1,3}S$ Feshbach resonances decrease rapidly when they approach the $2s$ threshold before they merge with the parent $2s$ state. The widths of $^{1,3}P$ Feshbach resonances also considerably decrease when they approach the $2s$ threshold, but after passing it their widths start to increase rapidly, a signature of the shape resonance (see the D dependence of the $^1P^\circ(2)$ shape resonance in Fig. 3). The phenomenon of transformation of a $^{1,3}P$ Feshbach resonance into a shape resonance has been discussed in detail in Ref. [10]. As argued there, this change of the character of the $^{1,3}P^\circ$ resonances results from two facts: the quasidegeneracy of $2s$ and $2p$ thresholds, in which case the two-electron states are described by the superpositions $\chi^S_\pm = 2snp \pm (-1)^S 2pns$ (S is the total electron spin) and the pronounced diffuse character of $2p$ state for the relative small values of D. In the hyperspherical coordinate representation, the states $\chi^S_\pm$ are eigenstates of the adiabatic hyperspherical Hamiltonian [30], to which adiabatic channel potentials $U^S_\pm$ are associated. As shown in Ref. [31] for $^1P^\circ$ states in the unscreened case, the hyperspherical potential $U^{S=0}_-$ supports only bound states below the $n = 2$ threshold [corresponding to the $^1P^\circ(1)$ Feshbach resonance], while the potential $U^{S=0}_+$ is not strong enough to support bound states but exhibits a potential barrier above the threshold which supports a quasibound state [corresponding to the $^1P^\circ(2)$ shape resonance]. In the screened case, because with decreasing D the wave functions become more and more diffuse, the $2p$ state can also mix with higher l states. Having in mind that for finite D the $2s$ and $2p$ thresholds are separated, this mixing produces a barrier in the $U^{S=0}_-$ potential. Therefore, after passing the $2s$ threshold the $^1P^\circ(1)$ state is prone to underbarrier decay (i.e., becomes a shape resonance). The mixing of $2p$ state with the d states is also responsible for the change of character of $^3P^\circ(1,2)$ resonances related to the hyperspherical potential $U^{S=1}_+$. The critical screening lengths, D_c, for which the Feshbach resonances $^1P^\circ(1)$, $^3P^\circ(2)$, and $^3P^\circ(1)$ pass the $2s$ threshold, lie in the regions 30–29 a.u., 48–45 a.u., and 6.3–6.2 a.u., respectively. The rapid increase of the widths of these resonances for $D < D_c$ observed in Fig. 3 is a consequence of the decrease of $2s$ threshold and the increase of diffuse character of bound and quasibound wave functions when D decreases.

The width of $^1D^e$ Feshbach resonance, for which the parent state is $2p$, in the region of D between the $2s$ and $2p$ thresholds (19 a.u. $\geqslant D \geqslant$ 14 a.u.) shows somewhat specific behavior: after passing the $2s$ threshold (in the region 19 a.u. $< D <$ 20 a.u.) it first continues to decrease (i.e., behaves like a Feshbach resonance with respect to the $2p$ threshold) and then starts to increase (i.e., behaves like a shape resonance with respect to the $2s$ threshold). Only after passing the $2p$ threshold in the region 13 a.u. $< D <$ 14 a.u., it behaves like a typical shape resonance with sharply increasing width. It has been argued in Ref. [10] that the behavior of the width of $^1D^e$ resonance before and after passing the $2p$ threshold can be taken as an indication of the existence of two barriers in the system of $U^{S=0}_\pm$ hyperspherical potentials. The $\chi^{S=0}_\pm$ superpositions for the $^1D^e$ resonance are made of the $2snd$ and $2pnp$ two-electron states.

The values of energy positions and widths of Feshbach and shape resonances parameters around $n = 2$ excitation threshold, as well as $2s$, $2p$ excitation threshold energies for a selected number of values of the screening length are given in Table III. It should be noted that the widths of shape resonances $^1P^\circ(2)$, $^3P^\circ(1)$, and $^1D^e$ become very large (larger than 0.015 Ry) for $D \leqslant 7$ a.u., $D \leqslant 4.2$ a.u., and $D \leqslant 5.0$ a.u., respectively, which makes their determination (as well as the determination of resonance positions) rather uncertain. It is interesting to note that the $^3P^\circ(1)$ shape resonance survives down to 3.8 a.u. (the last D value of our investigations), i.e., in the region $D < D_{2p} = 4.541$ a.u., where it exists as a quasibound state [32].

TABLE III. Feshbach and shape resonance parameters around n = 2 excitation threshold for a selected number of values of the screening length D (a.u.). E_r: resonance energy (Ry); Γ: resonance width (Ry); E_{th}: $2s$ or $2p$ excitation threshold (Ry).

D (a.u.)	∞		100		48		45		34	
	$2s$	$2p$	$2s$	$2p$	$2s$	$2p$	$2s$	$2p$	$2s$	$2p$
E_{th}(Ry)	0.750000	0.750000	0.749562	0.749658	0.748155	0.748555	0.747908	0.748360	0.746401	0.747172
$^{2s+1}L^{\pi}$	E_r	Γ	E_r	Γ	E_r	Γ	E_r	Γ	E_r	Γ
$^1S^e(1)$	0.702420	3.55(−3)	0.702370	3.55(−3)	0.702185	3.66(−3)	0.702110	3.52(−3)	0.701805	3.53(−3)
$^1S^e(2)$	0.747940	1.82(−4)	0.747791	1.85(−4)	0.747071	1.69(−4)	0.746918	1.60(−4)	0.745891	1.32(−4)
$^1S^e(3)$	0.749879	1.19(−5)	0.749532	6.54(−6)						
$^3S^e$	0.745763	1.40(−6)	0.745644	1.37(−6)	0.745085	1.28(−6)	0.744964	1.26(−6)	0.744146	1.16(−6)
$^1P^o(1)$	0.747883	2.77(−6)	0.747736	2.97(−6)	0.747068	3.15(−6)	0.746930	3.09(−6)	0.746006	2.72(−6)
$^1P^o(2)$	0.751120	1.72(−3)	0.750828	1.65(−3)	0.749921	2.09(−3)	0.749772	2.13(−3)	0.748856	2.34(−3)
$^3P^o(1)$	0.715760	4.32(−4)	0.715699	4.31(−4)	0.715447	4.35(−4)	0.715383	4.31(−1)	0.715003	4.31(−4)
$^3P^o(2)$	0.749176	1.02(−5)	0.748987	9.66(−6)	0.748114	6.52(−6)	0.747940	1.63(−5)	0.746772	4.25(−4)
$^1D^e$	0.744146	6.36(−4)	0.74404	6.32(−4)	0.743615	6.19(−4)	0.743527	6.16(−4)	0.742954	5.98(−4)
D (a.u.)	30		29		28		24		21	
	$2s$	$2p$	$2s$	$2p$	$2s$	$2p$	$2s$	$2p$	$2s$	$2p$
E_{th}(Ry)	0.745421	0.746397	0.745113	0.746153	0.744773	0.745884	0.742985	0.744463	0.740963	0.742850
$^{2s+1}L^{\pi}$	E_r	Γ	E_r	Γ	E_r	Γ	E_r	Γ	E_r	Γ
$^1S^e(1)$	0.701545	3.44(−3)	0.701465	3.43(−3)	0.701370	3.42(−3)	0.700860	3.39(−3)	0.700215	3.35(−3)
$^1S^e(2)$	0.745130	1.03(−4)	0.744882	9.44(−5)	0.744601	8.48(−5)	0.742984	1.12(−5)		
$^3S^e$	0.743552	1.08(−6)	0.743358	1.05(−6)	0.743138	1.02(−6)	0.741912	8.76(−7)	0.740388	6.88(−7)
$^1P^o(1)$	0.745326	2.07(−6)	0.745118	2.10(−6)	0.744854	2.81(−5)	0.74347	3.98(−4)	0.741944	1.09(−3)
$^1P^o(2)$	0.748086	2.30(−3)	0.747868	2.40(−3)	0.747641	2.51 (−3)	0.746432	3.06(−3)	0.745111	3.43(−3)
$^3P^o(1)$	0.714706	4.33(−4)	0.714615	4.33(−4)	0.714512	4.32(−4)	0.713936	4.29(−4)	0.713217	4.26(−4)
$^1D^e$	0.742540	5.85(−4)	0.742407	5.82(−4)	0.742258	5.77(−4)	0.74143	5.51(−4)	0.740413	5.20(−4)
D (a.u.)	20		19		18		17		14	
	$2s$	$2p$	$2s$	$2p$	$2s$	$2p$	$2s$	$2p$	$2s$	$2p$
E_{th}(Ry)	0.740090	0.742152	0.739085	0.741346	0.737918	0.740409	0.736551	0.739310	0.730695	0.734572
$^{2s+1}L^{\pi}$	E_r	Γ	E_r	Γ	E_r	Γ	E_r	Γ	E_r	Γ
$^1S^e(1)$	0.699920	3.34(−3)	0.699560	3.31(−3)	0.699195	3.52(−3)	0.698605	3.23(−3)	0.696160	3.09(−3)
$^3S^e$	0.739687	5.99(−7)	0.738843	4.89(−7)	0.737819	3.45(−7)	0.736539	1.84(−7)		
$^1P^o(2)$	0.744482	3.56(−3)	0.743755	3.68(−3)	0.742782	4.07(−3)	0.741745	4.16(−3)	0.737087	5.62(−3)
$^3P^o(1)$	0.712893	4.24(−4)	0.712490	4.21(−4)	0.712065	4.21(−4)	0.711453	4.15(−4)	0.708833	4.00(−4)
$^1D^e$	0.739955	5.05(−4)	0.739402	4.87(−4)	0.738754	4.71(−4)	0.737962	4.81(−4)	0.734334	5.97(−4)
D (a.u.)	13		12		10		8		6.3	
	$2s$	$2p$	$2s$	$2p$	$2s$	$2p$	$2s$	$2p$	$2s$	$2p$
E_{th}(Ry)	0.727864	0.732265	0.724357	0.729395	0.714260	0.721047	0.696676	0.706221	0.668864	0.681968
$^{2s+1}L^{\pi}$	E_r	Γ	E_r	Γ	E_r	Γ	E_r	Γ	E_r	Γ
$^1S^e(1)$	0.694855	2.96(−3)	0.69321	2.92(−3)	0.687865	2.66(−3)	0.677199	2.17(−3)	0.657593	1.47(−3)
$^1P^o(2)$	0.734962	4.53(−3)	0.732222	6.80(−3)	0.723832	8.81(−3)	0.708455	0.01226		
$^3P^o(1)$	0.707468	3.94(−4)	0.705686	3.83(−4)	0.700136	3.49(−4)	0.689110	2.90(−4)	0.668765	1.62(−4)
$^1D^e$	0.732359	6.38(−4)	0.729892	1.12(−3)	0.72259	2.96(−3)	0.709187	6.99(−3)	0.686261	0.01037
D (a.u.)	6.2		6		5		4.55		3.8	
	$2s$	$2p$	$2s$	$2p$	$2s$	$2p$	$2s$	$2p$	$2s$	–
E_{th}(Ry)	0.666582	0.679928	0.661710	0.675551	0.629405	0.645422	0.608681	0.624461	0.559754	–
$^{2s+1}L^{\pi}$	E_r	Γ	E_r	Γ	E_r	Γ	E_r	Γ	E_r	Γ
$^1S^e(1)$	0.655859	1.41(−3)	0.652093	1.30 (−3)	0.625312	6.54(−4)	0.606882	3.65(−4)	0.559720	1.49(−5)
$^3P^o(1)$	0.666944	2.31(−4)	0.662843	5.91(−4)	0.635203	6.15(−3)	0.616835	9.91(−3)	0.570664	0.02187
$^1D^e$	0.685216	0.01079	0.680200	0.01143	0.647662	0.01484				

IV. DYNAMIC EVOLUTION OF EXCITATION AND ELASTIC COLLISION STRENGTHS IN THE REGION AROUND THE $N = 2$ THRESHOLDS

The pronounced variation of the resonance parameters when the screening length of the potential varies (see Figs. 2 and 3) will obviously produce significant changes in the collision strengths of both excitation and elastic processes in the energy region around the $n = 2$ thresholds.

A. $1s \rightarrow 2s$ excitation collision strength

The dynamical evolution of $1s \rightarrow 2s$ excitation collision strength for a selected number of values of the screening length

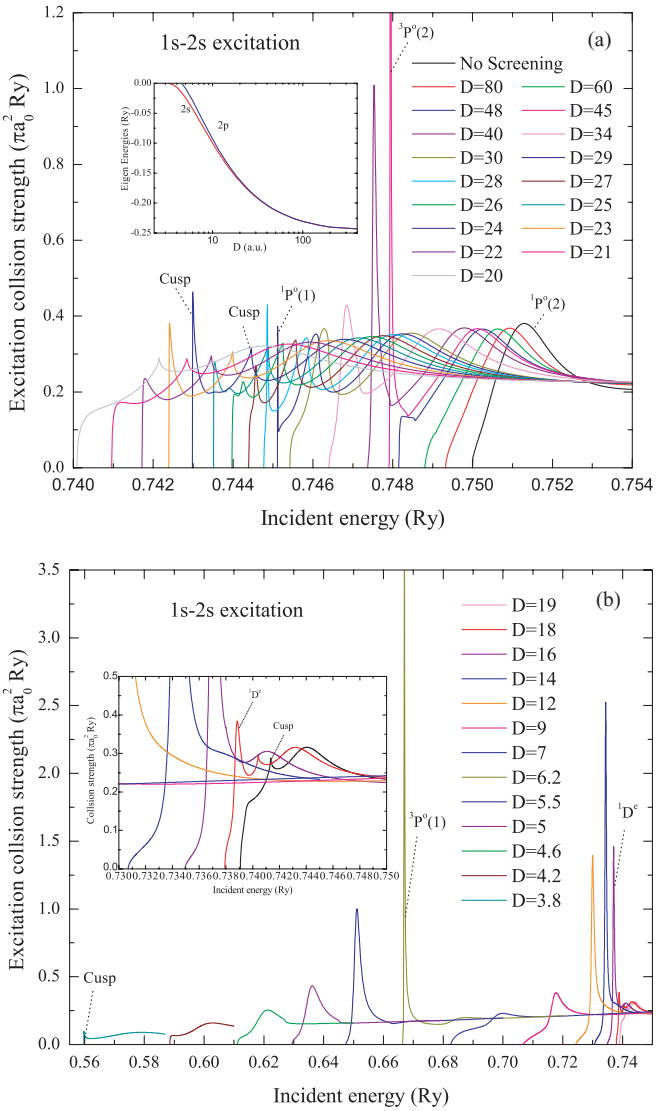

FIG. 4. (Color online) Dynamic evolution of $1s \rightarrow 2s$ collision strength when the screening length D decreases from $D = \infty$ to $D = 3.8$ a.u.. $^{2s+1}L^{\pi}(n)$ denotes the dominant resonance (The screening length increases from left to right).

between $D = \infty$ and $D = 3.8$ a.u. is shown in Figs. 4(a) and 4(b). In the inset of Fig. 4(a) the binding energies of $2s$ and $2p$ states are shown when D varies. Figure 4(a) shows that the maximum of the $1s \rightarrow 2s$ collision strength decreases with decreasing D as long as some of the Feshbach resonances contributing to the collision strength. This decrease is related to the decrease of the amplitudes of $1s$ and $2s$ wave functions with decreasing D (see, e.g., Ref. [12]), which also results in broadening of the half-width of the maximum of collision strength. The shift of the maximum of the collision strength to lower energies when D decreases is consistent with the shift of energy positions of all contributing resonances with decreasing D (see Fig. 2).

The most significant changes in the structure and values of $1s \rightarrow 2s$ collision strength, however, take place in the regions of D where $^{1,3}P$ and ^1D Feshbach resonances change their character. Thus, the sharp peak in the collision strength in Fig. 4(a) for $D = 45$ a.u. at $E_r = 0.74794$ Ry corresponds to the $^3P^{\circ}(2)$ resonance just after its transformation to shape resonance. With decreasing D, this peak moves to lower energies, its half-width becomes larger (see the curves for $D = 40$ and 34 a.u.), in accordance with the parameters of this resonance shown in Figs. 2 and 3, and its amplitude decreases rapidly.

The contribution of $^1P^{\circ}(1)$ resonance to the collision strength is generally small (see Fig. 4), but it still produces the clearly visible sharp peaks in the collision strength curves for $D = 29$ and 28 a.u. at $E_r = 0.745118$ Ry and $E_r = 0.744854$ Ry, respectively. The sharp peak in the collision strength in Fig. 4(b) for $D = 6.2$ a.u. at $E_r = 0.666944$ Ry is due to the new born $^3P^{\circ}(1)$ shape resonance resulting from the transformed $^3P^{\circ}(1)$ Feshbach resonance at the $2s$ threshold (lying somewhere between 6.3 and 6.2 a.u.). The amplitude of this resonance decreases rapidly with decreasing D, with its width increasing also rapidly (see also Fig. 3). This resonance dominates the $1s \rightarrow 2s$ collision strength for $D \leqslant 6.2$ a.u..

The sharp peaks on the right-hand-side of Fig. 4(b) are due to the $^1D^e$ resonance contribution, which acquires its maximum amplitude for $D = 14$ a.u. and then starts to decrease with decreasing D, disappearing in the background for $D < 7$ a.u..

The relatively small but sharp peaks (cusps) observed in the collision strength (see Fig. 4) represent the effects of virtual states [33]. The cusps seen in the collision strengths for $D = 19$ a.u. and $D = 18$ a.u. [see the inset in Fig. 4(b)] are related to the effect of virtual $^1P^{\circ}$ state. Similar virtual state effects appear also in the $^1S^e$ channel for $D \leqslant 27$ a.u. and $D \leqslant 4$ a.u., as can be observed in Figs. 4(a) and 4(b), respectively. Virtual states above the 2s threshold appear in the $^3P^{\circ}$ and $^1P^{\circ}$ channels for $D \leqslant 34$ a.u. [see Fig. 4(a)] and $D \leqslant 21$ a.u. [see Figs. 4(a) and 4(b)], respectively. For some D values more than one cusp can be seen in the collision strength (e.g., for $D = 24$, 23 and 22 a.u.).

The effects of virtual states in the collision strength is illustrated in Fig. 5, where the $1s \rightarrow 2s$ partial wave collision strength of S, P, and D waves (upper panel) and their eigenphase sums (lower panel) are shown for $D = 24$ a.u.. There are four virtual states for this value of D in the considered energy range: $^1S^e$ and $^3S^e$ at the $2s$ excitation threshold and

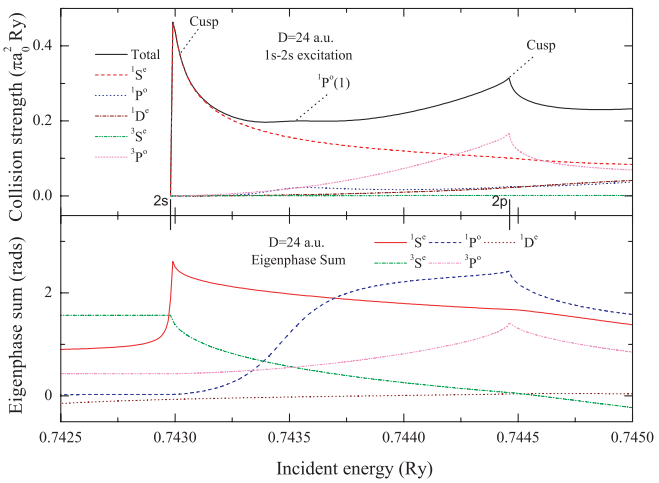

FIG. 5. (Color online) Eigenphase sum and $1s \rightarrow 2s$ partial wave collision strengths for S, P and D waves for $D = 24$ a.u..

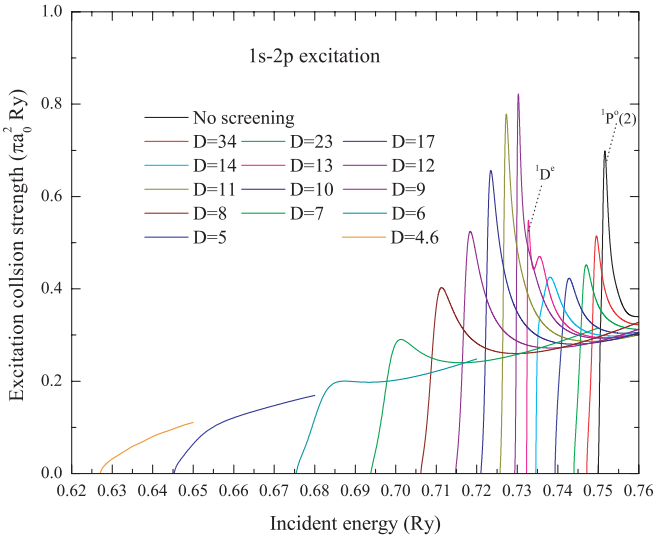

FIG. 6. (Color online) Dynamic evolution of $1s \rightarrow 2p$ collision strength when the screening length D decreases from $D = \infty$ to $D = 4.6$ a.u. (The screening length increases from left to right).

$^1P^\circ$ and $^3P^\circ$ at the $2p$ excitation threshold. It can be seen from the lower panel of this figure that the eigenphase sum of the $^1S^e$ Feshbach resonance is cut short at the $2s$ threshold due to the opening of $2s$ channel; this produces a peak in the $1s \rightarrow 2s$ collision strength just above the $2s$ excitation threshold. On the other hand, the $^3P^\circ$ Feshbach resonance is totally destroyed by the virtual state for partial wave $^3P^\circ$, which can be clearly observed as a cusp peak in the $1s \rightarrow 2s$ collision strength at the $2p$ excitation threshold (at $E = 0.74481$ Ry).

We should note that similar virtual state effects have also been observed in the electron–helium excitation cross sections in the $n = 2$ thresholds region [34,35], where the Coulomb degeneracy is lifted. However, while in the helium atom case the $n = 2$ level splitting is fixed, the screened potential (1) contains a continuously varying parameter that allows us to study the effects of the screening on the resonances and virtual states near $n = 2$ excitation thresholds to the full extent.

B. $1s \rightarrow 2p$ excitation collision strength

Dynamical evolution of the $1s \rightarrow 2p$ excitation collision strength for a number of selected screening lengths between $D = \infty$ and $D = 4.6$ a.u. is shown in Fig. 6. Only two resonant states contribute to the $1s \rightarrow 2p$ collision strength in the considered energy range: the $^1P^\circ(2)$ shape resonance for $D > 14$ a.u. and the $^1D^e$ shape resonance for $D \leqslant 13$ a.u.. The amplitude of the $^1D^e$ resonance acquires its maximum at $D = 12$ a.u.. For the smaller D values, the $^1D^e$ resonance peak decreases rapidly (its half-width becoming increasingly larger) and for $D = 5$ a.u., it disappears into the background.

C. $1s \rightarrow 1s$ elastic collision strength

The $1s \rightarrow 1s$ elastic collision strength below the $n = 2$ excitation threshold when the screening length D decreases from $D = \infty$ to $D = 3.8$ a.u. is shown in Fig. 7. The dominant resonances and cusps are also marked in the figures. The significant changes in the structure and values of the collision strength are obviously related to the changes of the resonance parameters when D decreases.

As Fig. 7(a) shows, the Feshbach $^1S^e(3)$ resonance gives an important contribution to the elastic collision strength. However, when D becomes less than 100 a.u., this resonance converges to its parent state $2s$ and virtual state begins to play important role in the elastic collision near the $2s$ threshold. This virtual state manifests itself as a cusp in the collision strength. With the further decrease of D this cusp merges into the background. A similar behavior shows also the $^1S^e(2)$ Feshbach resonance [see Figs. 7(a) and 7(b)]; the cusp appears after $^1S^e(2)$ merges with the $2s$ threshold, i.e., when D is less than 24 a.u.. Furthermore, Figs. 7(a)–7(e) show that the $^1S^e(1)$ Feshbach resonance plays important role in the elastic process in the entire range of screening lengths considered here.

It should be noted that the $^3S^e$ Feshbach resonance is very narrow and does not contribute significantly to the collision strength. When D becomes less than 22 a.u., the $^3S^e$ merges into the huge background of the $^1D^e$ resonance having a close resonance position with $^3S^e$.

The contribution of $^3P^o$ (2) Feshbach resonance to the elastic collision strength is also significant, but it decreases rapidly when D becomes smaller than 48 a.u. [see Figs. 7(a) and 7(b)] when it transforms into shape resonance. After this transition, the width of $^3P^o$ (2) resonance increases rapidly with decreasing D and the associated peak in the collision strength becomes increasingly broader. When D becomes smaller than about 34 a.u., the $^3P^o$ (2) resonance disappears into the background.

The positions of $^1P^o$ (1) and $^1S^e(2)$ Feshbach resonances are very close to each other but the width of the former is much smaller than that of the latter for all D before $^1P^o$ (1) transforms into a shape resonance at about $D = 29$ a.u. (see Figs. 2 and 3). The $^1P^o$ (1) narrow contribution peak in collision strength is superimposed to the broad contribution peak of $^1S^e(2)$. After $^1P^o$ (1) changes its character (at $D \approx 29$ a.u.), its contribution to the collision strength becomes very small and is immersed into the broad peak of $^1S^e(2)$.

Figures 7(d) and 7(e) show that the contribution of $^3P^\circ(1)$ Feshbach resonance to the collision strength is very significant and quasiunchangeable with decreasing D until it undergoes a change of its character at about $D = 6.3$ a.u.. After this transition, its contribution to the collision strength decreases rapidly and with the further decrease of D it immerses into the background and disappears.

As Figs. 7(a)–7(c) show, the $^1D^e$ Feshbach resonance also gives a significant and quasi-invariable contribution to the elastic collision strength when D decreases until it passes across the $2s$ threshold at about $D = 20$ a.u.. With the further decrease of D in the range 19 a.u. $\geqslant D \geqslant 14$ a.u., the contribution of this resonance to the collision strength gradually decreases [see Fig. 7(c)]. At $D \approx 14$ a.u., the $^1D^e$ resonance passes across the $2p$ threshold and becomes a typical shape resonance; its contribution to the collision strength quickly merges into the background with the further decrease of D, as observed in Fig. 7(c). The observed quasi-invariant contribution of $^1D^e$ Feshbach resonance to the elastic

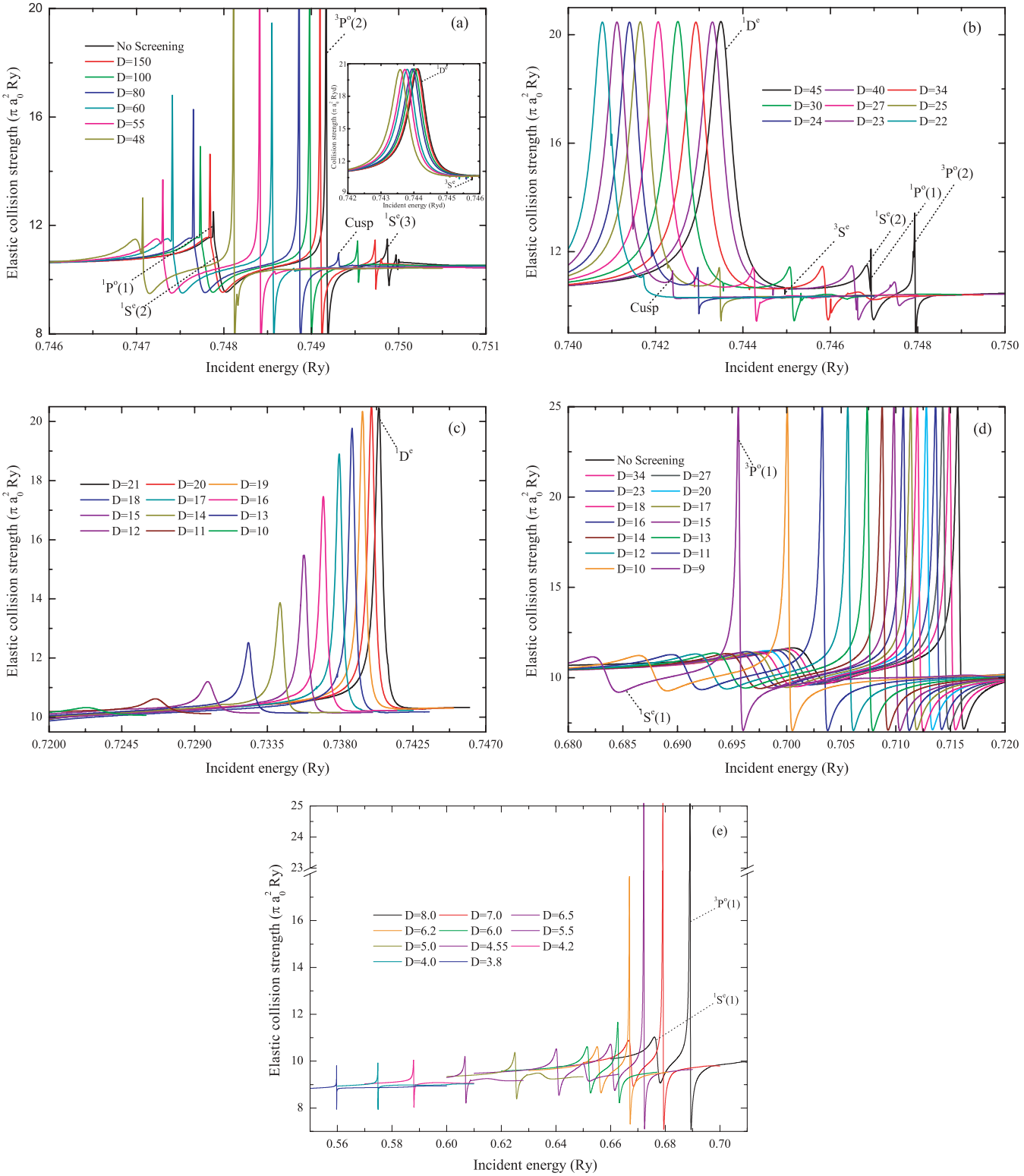

FIG. 7. (Color online) Dynamic evolution of $1s \rightarrow 1s$ elastic collision strength when the screening length varies from $D = \infty$ to $D = 3.8$ a.u.. $^{2s+1}L^{\pi}(n)$ denotes the dominant resonance (The screening length increases from left to right).

collision strength for $D \geqslant 20$ a.u. is a consequence of the diffuse character of dominant one-electron states involved in two-state configuration mixing which are less sensitive to the variation of D.

We note that for $D \leqslant 6$ a.u., the elastic collision strength is dominated by the contribution from the $^1S^e$ (1) Feshbach resonance [see Fig. 7(e)]. We further note that for $D \leqslant 4.541$ a.u., only the $1s$ and $2s$ states remain in the discrete

spectrum of H atom [12] and, consequently, the doubly excited states resulting in Feshbach resonances must be of the S type.

V. CONCLUSIONS

In the present work we have studied the effects of screened Coulomb interaction on the electron–hydrogen-atom elastic and excitation scattering processes around the $n = 2$ excitation thresholds by using the RMPS method, modified for interactions of type (1). The lifting of the Coulomb l degeneracy by the potential screening (resulting in separation of $2s$ and $2p$ thresholds) and the decrease of the number of bound states in the screened Coulomb potential (resulting in reduction of the number of resonant states) profoundly affect the dynamics of near-threshold elastic and excitation processes. Furthermore, the phenomenon revealed in Ref. [10] of transformation of Feshbach $^{1,3}P$ and ^{1}D resonances to shape-type resonances when the screening length D crosses over the $2s$ and $2p$ threshold, respectively, dramatically affects the dynamical evolution of elastic and excitation collision strengths when D varies. These changes are related to the changes of the positions and widths of resonances when D varies, for which we presented a detailed information in the range $D = \infty$ to 3.8 a.u., obtained by using the eigenphase sum method. With decreasing D the energy position of resonances decreases. Their widths also decrease with decreasing D, particularly sharply for the $^{1,3}S$ resonances, when they approach the $2s$ threshold for a certain D value, but those of $^{1,3}P$ and ^{1}D resonances increase sharply after they become shape resonances by crossing the corresponding threshold at certain critical value of D.

The evolution of elastic and $1s \rightarrow 2s$, $1s \rightarrow 2p$ excitation collision strengths in the near-threshold energy region is presented in the range $D = \infty$ to 3.8 a.u.. The significant changes observed in the structure and magnitude of collision strengths as D varies (see Figs. 4, 6, and 7), a result of the convergence of $^{1,3}S$ Feshbach resonances to the varying $2s$ threshold and the transformation of $^{1,3}P$ and ^{1}D Feshbach resonances into shape-type resonances when they pass across the $2s$ and $2p$ threshold at certain critical value of D, respectively. We mention that cusps in the collision strengths appear when the $^{1,3}S$ and $^{1,3}P$, ^{1}D resonances approach the $2s$ and $2p$ threshold, respectively.

The electron–hydrogen-atom elastic and excitation collision processes with screened Coulomb interactions in the $n = 3$ resonant energy region will be considered in forthcoming papers.

ACKNOWLEDGMENTS

This work has been partly supported by the National Natural Science Foundation of China (Grant Nos. 10974021, 10875017, 10774186, and 10876043), the National Key Laboratory of Computational Physics Foundation (No. 9140C6904030808), and the CAS knowledge promotion project (No. KJCX1-YW-N30).

[1] D. Salzman, *Atomic Physics in Hot Plasmas* (Oxford University Press, Oxford, 1998).
[2] M. S. Murillo and J. C. Weisheit, Phys. Rep **302**, 1 (1998).
[3] J. P. Hansen and I. R. McDonald, *Theory of Simple Fluids* (Academic, London, 1986).
[4] A. V. Vinogradov and V. P. Shevelko, Sov. Phys. JETP **44**, 542 (1976).
[5] B. L. Whitten, N. F. Lane, and J. C. Weisheit, Phys. Rev. A **29**, 945 (1984); **30**, 650 (1984).
[6] J. K. Yuan, Y. S. Sun, and S. T. Zheng, J. Phys. B **29**, 153 (1996).
[7] Y.-D. Jung, Phys. Plasmas **2**, 332 (1995); **2**, 1775 (1995); **4**, 21 (1997).
[8] Y. Y. Qi, Y. Wu, J. G. Wang, and Y. Z. Qu, Phys. Plasmas **16**, 023502 (2009).
[9] Y.-D. Jung and J.-S. Yoon, J. Phys. B **29**, 3549 (1996).
[10] S. B. Zhang, J. G. Wang, and R. K. Janev, Phys. Rev. Lett. **104**, 023203 (2010).
[11] L. D. Landau and E. M. Lifshitz, *Quantum Mechanics: Non-Relativistic Theory* (Pergamon, London, 1958).
[12] F. J. Rogers, H. C. Graboske, and D. J. Harwood, Phys. Rev. A **1**, 1577 (1970).
[13] P. G. Burke, A. Hibbert, and W. D. Robb, J. Phys. B **4**, 153 (1971).
[14] P. G. Burke, C. J. Noble, and V. M. Burke, Adv. At. Mol. Phys. **54**, 237 (2007).
[15] C. J. Joachain, *Quantum Collision Theory* (North-Holland, Amsterdam, 1975), p. 670.
[16] F. Salvat, J. M. Fernfindez-Varea, and W. Williamson Jr, Comput. Phys. Commun. **90**, 151 (1995).
[17] A. Hibbert, Comput. Phys. Commun. **9**, 141 (1975).
[18] K. A. Berrington, W. B. Eissner, and P. H. Norrington, Comput. Phys. Commun. **92**, 290 (1995).
[19] Modified version of RMATRIX I, http://amdpp.phys.strath.ac.uk/rmatrix/.
[20] H. Friedrich, *Theoretical Atomic Physics*, 3rd ed. (Springer, Berlin, 2006), p. 47.
[21] K. M. Dunseath, M. Terao-Dunseath, and J.-M. Launay, J. Phys. B **33**, 3037 (2000).
[22] J. Callaway, Phys. Lett. A **81**, 495 (1981).
[23] J. Callaway, Phys. Rev. A **26**, 199 (1982).
[24] T. T. Gien, J. Phys. B **31**, L1001 (1998).
[25] P. G. Bruke and A. J. Taylor, Proc. R. Soc. London **88**, 549 (1966).
[26] M. K. Chen, C. D. Lin, and J. Z. Tang, Phys. Rev. A **56**, 2435 (1997).
[27] Y. D. Wang, W. C. Fon, and C. D. Lin, J. Phys. B **29**, L59 (1996).
[28] K. Bartschat, I. Bray, P. G. Burke, and M. P. Scott, J. Phys. B **29**, 5493 (1996).
[29] J. F. Willams, J. Phys. B **9**, 1519 (1976).
[30] C. D. Lin, Adv. At. Mol. Phys. **22**, 77 (1986).
[31] C. D. Lin, Phys. Rev. Lett. **35**, 1150 (1975).
[32] M. Bilycki, A. Stachov, J. Karwowski, and P. K. Mukherjee, Chem. Phys. **331**, 346 (2007).
[33] P. G. Burke, J. W. Cooper, and S. Ormonde, Phys. Rev. **183**, 245 (1969).
[34] K. A. Berrington, P. G. Burke, and A. L. Sinfailam, J. Phys. B **8**, 1459 (1975).
[35] E. T. Hudson, K. Bartschat, M. P. Scott, P. G. Burke, and V. M. Burke, J. Phys. B **29**, 5513 (1996).